

7. R. Liepins *et al.*, *J. Vac. Sci. Technol.* **18**, 1218 (1981).
8. L. A. Scott, R. G. Schneggenburger, and P. R. Anderson, *J. Vac. Sci. Technol. A* **4**, 1155 (1986).
9. P. C. Souers, *Hydrogen Properties for Fusion Energy* (University of California Press, Berkeley, CA, 1986), p. 371.
10. *Ibid.*, p. 370.
11. M. D. Wittman, D. Malacara, and H.-J. Kong, in *Laser Interferometry IV: Computer-Aided Interferometry* (SPIE, Bellingham, WA, 1991), Vol. 1553, p. 456.
12. R. L. Woerner and T. J. Greytak, *Rev. Sci. Instrum.* **47**, 383 (1976).
13. R. Wallenstein and T. W. Hänsch, *Appl. Opt.* **13**, 1625 (1974).
14. *International Critical Tables of Numerical Data, Physics, Chemistry and Technology*, edited by E. W. Washburn (McGraw-Hill, New York, 1930), Vol. VII, pp. 1–12.

## 2.C Raman Scattering of High-Power Lasers in Air

Inertial-confinement laser fusion requires propagation of high-intensity, pulse-shaped IR and UV laser beams through long air paths. Such beams are subject to losses and decreased beam quality because of stimulated rotational Raman scattering (SRRS) in the atmosphere. With short pulses, it is necessary to use transient Raman theory to include buildup and relaxation of the medium. Imperfect beam quality can lead to intensity hot spots that change the effective threshold for Raman scattering. A detailed analysis of energy conversion and beam quality necessitates a four-dimensional (4-D) treatment of the laser pump, the Stokes beam, and the air path. The SRRS model includes laser pulse shape, medium excitation and relaxation, and spontaneous scattering as a quantum initiation of the Stokes field.

Typical irradiance levels for the OMEGA Upgrade laser system are  $\sim 2 \text{ GW/cm}^2$ , giving a steady-state gain length of about 60 cm. Depending on the particular system configuration, an air path of between 15 m and 20 m may be required, corresponding to as much as approximately 30 gain lengths. Fortunately, the transient Raman gain may be considerably less than the steady-state gain. However, the problem is exacerbated by intensity nonuniformities in the laser beam. These hot spots are common in the near field, arising from diffraction propagation of high-frequency aberrations. Raman conversion of the laser to Stokes light is enhanced at the location of hot spots, leading to a change in the overall Raman conversion.

The Stokes radiation generated in the air path arises from spontaneous Raman scattering and is subsequently amplified by stimulated Raman scattering. The origin of spontaneous Raman scattering is a low-level random polarization of the

nitrogen molecule in the air caused by quantum fluctuations. The quantum-induced medium polarization is uncorrelated spatially, referred to as delta-correlated spatially. The laser scatters off the delta-correlated polarization sites to produce Stokes light that spreads in all directions. Only the Stokes light that is primarily in the forward direction receives appreciable stimulated amplification, so we are justified in ignoring the Stokes light scattered backward and to the sides. However, the angle of the Stokes light in the forward direction, which is amplified, is still of substantial size. The solid angle of effective stimulated amplification is determined by the area of the beam divided by square of the length, which is of the order of 0.1–0.2 msterad for the OMEGA Upgrade laser system. This wide-angle Stokes radiation does not reach the fusion target in the far field, so the Raman process is a parasitic process causing beam-to-beam power imbalance. Since the rate of Stokes generation is very strongly dependent on hot spots, it is necessary to include two-dimensional (2-D) diffraction propagation of both the laser and Stokes fields. The wide-angle Stokes light requires high sampling densities leading to the need for large arrays, which make diffraction calculations difficult. Arrays of  $1024 \times 1024$  or larger may be required, leading to a significant computational problem.

The need to treat the transient response of the medium compounds the computational difficulties. The medium responds to the radiation with a characteristic response time of 133 ps. A typical laser pulse is about 700 ps in length. It is necessary to resolve the medium response time over the course of the pulse, leading to the requirement of several hundred time samples, each of which requires diffraction and kinetic calculations for the large arrays.

To further add to our difficulties it is necessary to represent the state of the medium (air) at many axial positions with the same array size as the typical beams. Fortunately, it is not necessary to fully resolve the 32 gain lengths with axial samples. To the extent that the governing medium equations are at least piece-wise analytically described, the axial spacing may be extended. Instead of the several hundred axial samples needed to resolve a maximum of 32 gain lengths, only about 30–40 axial samples will suffice. In order of importance, we seek to minimize the size of the arrays because of diffraction calculations, the number of medium arrays, and finally the number of time steps.

### Physics of Stimulated Raman Scattering

In light of the practical difficulties imposed by the high sampling requirements, both transverse and axial, and the large temporal-sampling necessities, the numerical methods must be designed with optimum computational efficiency. To apply the Raman model to the laser-fusion application, it is necessary to incorporate the model into a comprehensive system-analysis program capable of modeling all components, aberrations, diffraction propagation, etc. The laser analysis program GLAD was chosen for this purpose. GLAD operates on a variety of computers ranging from IBM PCs to Cray supercomputers.<sup>1</sup>

The governing Raman equations are<sup>2</sup>

$$\left[ \nabla_{\perp}^2 + 2ik_L \frac{\partial}{\partial z} \right] E_L = 2k_3 k_L Q E_s, \quad \text{laser depletion,} \quad (1)$$

$$\left[ \nabla_{\perp}^2 + 2ik_S \frac{\partial}{\partial z} \right] E_S = 2k_2 k_S Q^* E_L, \quad \text{Stokes amplification, and} \quad (2)$$

$$\frac{\partial Q^*}{\partial t} = -\Gamma Q^* + ik_1 E_L^* E_S + F^*, \quad \text{medium nonlinear polarization,} \quad (3)$$

where  $E_L$  and  $E_S$  are the laser and Stokes complex amplitudes and  $Q$  is the medium polarization. The respective wave numbers are  $k_L$  and  $k_S$ . The gain medium constants are  $k_1, k_2$ , and  $k_3$ .  $\Gamma$  is the Raman bandwidth and  $F$  is a delta-correlated random force representing random dephasing caused by collisions. Equations (1) and (2) define the diffraction propagation and the effect of the medium polarization  $Q$  on the optical fields  $E_L$  and  $E_S$ . Equations (1) and (2) are expressed in a coordinate system moving at the speed of light. Equation (3) defines the temporal behavior of the medium polarization in terms of the product of the optical fields and the random collisional force  $F$ . Solution of these three equations has been extensively explored in the literature under various approximations. References 2, 3, and 4 are representative. References 5 and 6 describe some of the interesting experiments that have been conducted.

The form of the exact solution, including diffraction, but neglecting pump depletion, invokes a three-dimensional convolution in space and a convolution in time. While the solution is elegant, the spatial and temporal convolutions are very difficult to implement for the numerous large arrays needed to describe the optical fields and the medium polarization. This solution has been most readily applied to very low Fresnel-number problems. In our application, Fresnel numbers of about 10,000 are typical and the difficulties of direct Green's-function solutions are more serious.

We elected to develop our model from the basic differential equations. We may separate the diffraction and the optical-field interactions with the medium using the split-step method.<sup>7,8</sup> This allows FFT methods to be used for diffraction propagation.

$$\frac{\partial E_L}{\partial z} = \frac{i}{2k_L} \nabla_{\perp}^2 E_L \quad (4)$$

represents diffraction for  $E_L$ , and

$$\frac{\partial E_S}{\partial z} = \frac{i}{2k_S} \nabla_{\perp}^2 E_S \quad (5)$$

represents diffraction for  $E_S$ . The medium polarization is influenced by stimulated Raman in the form of the product of the optical fields, the collisional force, and dephasing decay associated with collisions. Since Eq. (3) indicates a linear response of  $Q$  to the two driving forces, we may treat these separately.

$$\frac{\partial Q_{SRS}^*}{\partial t} = -\Gamma Q_{SRS}^* + ik_1 E_L^* E_S(z) \tag{6}$$

represents stimulated Raman amplification and decay, and

$$\frac{\partial Q_{SR}^*}{\partial t} = -\Gamma Q_{SR}^* + F^* \tag{7}$$

represents collision effects and decay. The collisional force  $F$  of Eq. (7) forms a random-scattering field, as shown in Fig. 52.21. The variance of random component  $Q_{SR}$  is constant, although the amplitude and phase at each point varies at the Raman response time. The spontaneous Raman scattering may be modeled as a mechanism for scattering the laser pump into the Stokes field according to a constant  $g_2$ . Spontaneous Raman scatters into all directions but we consider only the radiation scattered into the forward direction as defined by  $\Delta\Omega$ .

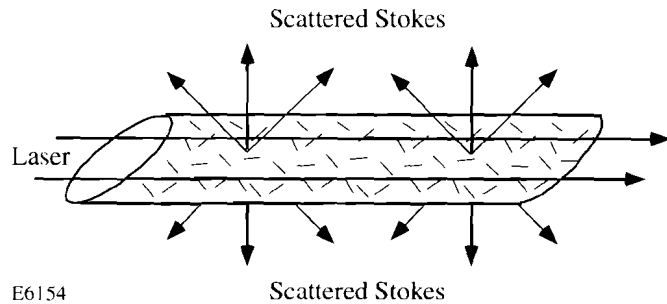


Fig. 52.21

A laser beam incident from the left is scattered by the medium field QSR, which is delta correlated spatially and scatters light into  $4\pi$  steradians. Only the light scattered in the forward direction contributes to the amplified Stokes.

The random element of spontaneous Raman is treated by a set of time-evolving random phasors at each point. The spontaneous emission noise takes the form

$$\langle I_S(x, y, z, +\Delta z, t_n) \rangle = \langle I_S(x, y, z, t_n) \rangle + g_2 I_L(t_n) \frac{\lambda^2}{4\pi\Delta x\Delta y} \Delta z, \tag{8}$$

where  $g_2$  is the spontaneous Raman-gain coefficient and can be determined by theoretical or experimental spontaneous Raman-scattering data, and  $I_L$  and  $I_S$  are the laser and Stokes irradiances. The factor  $\Delta\Omega = \lambda^2/\Delta x\Delta y$  is the maximum solid angle represented by a computer array with sampling intervals  $\Delta x$  and  $\Delta y$ .<sup>9</sup> This becomes of major importance when an angle of 10 mrad may need to be represented. This leads to very fine sampling densities and necessarily very large arrays. The effect of hot spots and extremely high amplification ameliorate this effect, to some degree making the effective Stokes source much narrower.

The random noise is introduced by the use of a spatially uncorrelated random variable  $X$ , which is a unit variance complex random number, normally distributed in amplitude and uniformly distributed in phase, represented by

$$E_S(x, y, z + \Delta z, t_n) = E_S(x, y, z, t_n) + \left[ g_2 I_L(x, y, z, t_n) \frac{\Delta \Omega}{4\pi} \Delta z \right]^{1/2} X(x, y, z, t_n). \quad (9)$$

To include the finite temporal correlation, we update the random number with a second random number  $Y$

$$X(x, y, z, t_n) = X(x, y, z, t_{n-1}) e^{-\Gamma \Delta t} + Y(x, y, z, t_n) \left( 1 - e^{-2\Gamma \Delta t} \right)^{1/2}. \quad (10)$$

Having considered diffraction and spontaneous Raman scattering by means of separate split-step operations, we need only add the stimulated Raman amplification

$$\frac{\partial E_L}{\partial z} = ik_3 Q E_S, \quad (11)$$

$$\frac{\partial E_S}{\partial z} = -ik_2 Q^* E_L, \quad (12)$$

$$\frac{\partial Q^*_{SRS}}{\partial t} = -\Gamma Q^*_{SRS} + ik_1 E_L^* E_S(z). \quad (13)$$

Carmen *et al.*<sup>4</sup> give a closed-form expression for stimulated Raman amplification (ignoring pump depletion and diffraction)

$$E_S(z, t) = E_S(0, t) + (k_1 k_2 z)^{1/2} E_L(t) \int_{-\infty}^t e^{-\Gamma(t-t')} \left\{ E_L^*(t') E_S(0, t') [\tau(t) - \tau(t')]^{-1/2} I_1 \left( 2 \left[ k_1 k_2 z [\tau(t) - \tau(t')] \right]^{1/2} \right) \right\} dt', \quad (14)$$

where

$$\tau(t) = \int_{-\infty}^t |E_L(t')|^2 dt'. \quad (15)$$

This approach requires that we save the temporal functions  $E_L^*(t') E_S(0, t')$  and  $\tau(t)$  over several response times for each transverse point and for each axial sample. If we neglect diffraction, then one axial point suffices. However, to treat the diffraction-induced hot spots, we need to have axial samples every 0.5 m to 2 m. Hence, Eq. (14) leads to the need to manipulate a very large amount of data.

Since we need a reasonable number of axial samples, we may simply solve Eqs. (12) and (13) directly. We store the time-integrated value  $Q^*$ ;

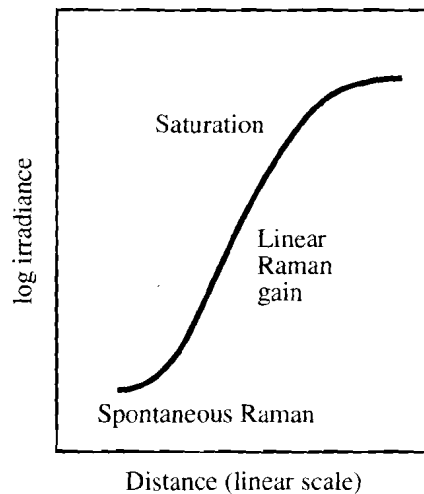
$$Q_{SRS}^*(z, t) = ik_1 \int_{-\infty}^t e^{-\Gamma(t-t')} E_L^*(z, t') E_S(z, t') dt'. \quad (16)$$

Because of the particular form of  $e^{-\Gamma(t-t')}$ , we do not have to save the time history of the product of  $E_L^*(z, t') E_S(z, t')$  and can save only  $Q_{SRS}^*(z, t)$  according to the evolving sum

$$Q_{SRS}^*(z, t + \Delta t) = Q_{SRS}^*(z, t) e^{-\Gamma \Delta t} + ik_1 e^{-\Gamma \Delta t} E_L^*(z, t) E_S(z, t), \quad (17)$$

where  $\Delta t$  is the temporal sampling.

We now integrate Eq. (12) through the axial samples to find  $E_S$ , including diffraction, apertures, atmospheric aberration, and any other effects that exist between the axial samples.  $Q_{SRS}^*(z, t)$  varies rapidly with  $z$ , following a nearly exponential form. We make use of this nearly exponential property to reduce the number of axial samples required (see Fig. 52.22).



E6153

Fig. 52.22  
Semi-exponential growth of Stokes light in the spontaneous regime (shown schematically).

Equation (14) and our revised methods based on Eqs. (12) and (17) give essentially identical results. It is easier to see the variation of gain with distance from Eq. (14). In the transient regime, Eq. (14) shows a square-root dependence on distance.

The beam is characterized by Fresnel numbers of the order of 10,000. This implies that diffraction effects caused by the aperture are localized to the immediate vicinity of the aperture edge and may safely be neglected. The

aberration of the laser pump may have features as small as 1 cm or less. This aberration is relatively easy to resolve using an array of  $128 \times 128$  or larger. This type of aberration is the source of hot spots because of diffraction effects, but a centimeter-sized aberration structure forms strong hot spots over a distance of about 100 m or more but weaker hot spots over the 20-m beam path. However, diffraction in the upstream beam at smaller diameter can form hot spots over short distances, typical of a master oscillator power amplifier (MOPA) laser configuration.

The Stokes beam is characterized by very fine structure speckle. In the regime of no significant pump depletion, the amplification is linear. While spontaneous Raman light occurs throughout the entire beam path, the noise that is generated furthest upstream receives the most amplification and dominates the process. When viewed from the end of the beam path looking backward toward the start of the beam path (not recommended in practice for gigawatt beams) we would see a self-luminous fog of Stokes noise with the most upstream fog being brightest. One may consider the noise source to occur in the first gain length. The Stokes source is a delta-correlated coherent object and creates a speckle pattern with characteristic feature size of  $\lambda/\theta$ , where  $\theta$  is the subtense of the Stokes noise source as viewed by final Stokes field. The speckle size increases with beam path length but at 10 m the size is approximately  $23 \mu\text{m}$ , which is too small to be resolved. However, this speckle size assumes a perfectly uniform laser pump. In actuality, the laser will inevitably have some degree of nonuniformity of irradiance.

### OMEGA Upgrade Laser System

The OMEGA Upgrade laser project involves the enhancement of the existing OMEGA Nd:glass laser system for exploration of the ignition-scaling regime of inertial-confinement fusion (ICF) physics research. This project will result in a 30-kJ, 351-nm, 60-beam, direct-drive laser facility that features versatile pulse shaping using beam co-propagation and uniform target irradiation using broadband phase-conversion techniques. The schematic illustration in Fig. 52.23 shows the relationship between beam co-propagation and the continuous pulse shapes envisioned for the OMEGA Upgrade laser system.

The final infrared energy, produced by a series of rod and disk Nd:glass amplifiers arranged in a MOPA configuration, is frequency converted to the UV and then transported to the target chamber. The path length in air is minimized with a two-mirror-per-beamline configuration (Fig. 52.24) to reduce the distance

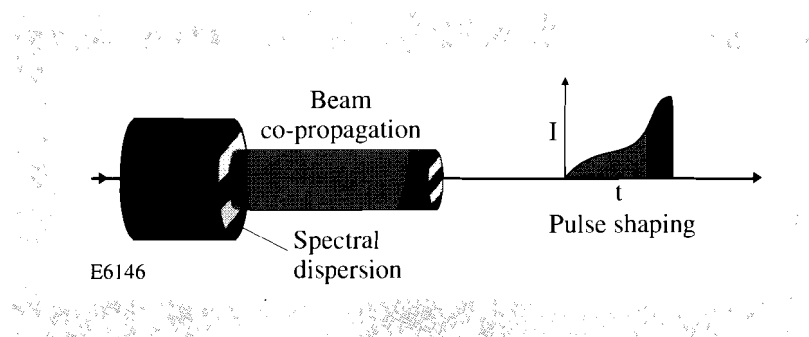
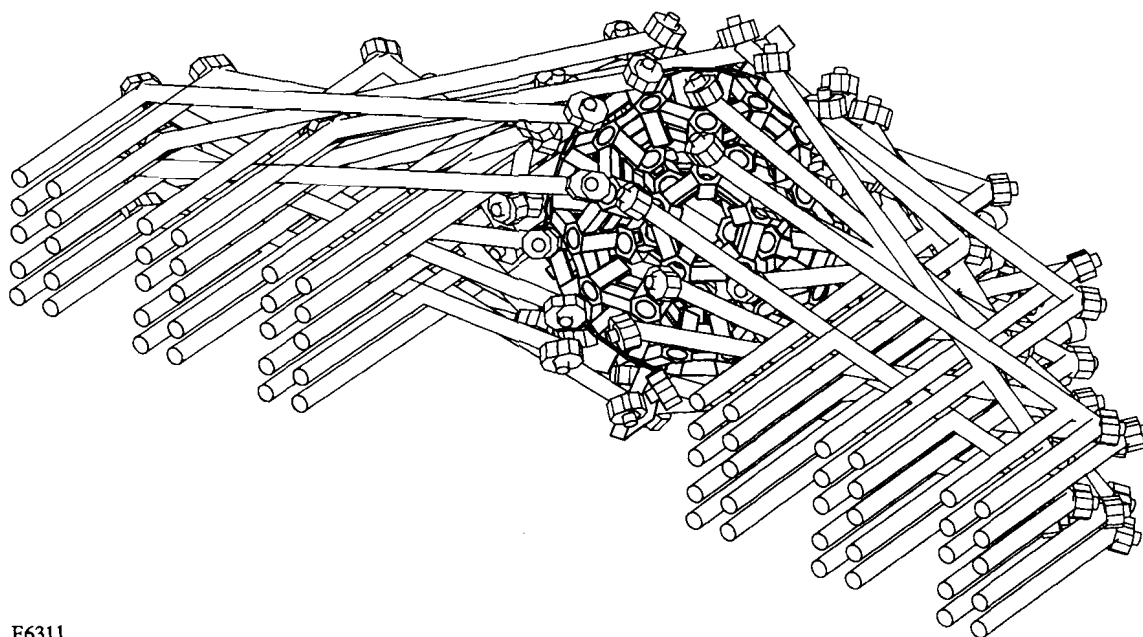


Fig. 52.23

The individual (inner and outer) portions of the co-propagated beam are electro-optically shaped to form the continuous pulse shape used in the OMEGA Upgrade laser system.



E6311

Fig. 52.24

The OMEGA Upgrade laser system includes an ultraviolet transport system that requires an 18-m path in air between the frequency-conversion cell and the final focus lens.

over which an intense beam propagates in a nitrogen-rich environment. Considerations of conversion efficiency, on-target energy balance, and system flexibility resulted in a propagation distance of  $\leq 20$  m between frequency-conversion cells and the focusing lens of the target chamber. Although preliminary estimates of SRRS efficiency showed that operation of the OMEGA Upgrade laser at full design energy remained below threshold for SRRS, further investigation of near-threshold operation is an important consideration for meeting performance requirements over the entire life of the laser.

The parameters used within this GLAD SRRS code are contained in Table 52.III. The peak laser-beam irradiance listed is consistent with the 30-kJ, full-system UV output. The gIL product, assuming steady-state gain, is approximately 25, which indicates near-threshold condition. However, the Gaussian and continuous pulse-shaped temporal profiles envisioned for use on the laser are short enough that below-threshold operation of the laser is predicted. Figures 52.25 and 52.26 illustrate the transient response to the baseline Gaussian and pulse-shaped temporal waveforms of the laser pump, respectively. The resulting Stokes temporal waveform follows the peak of the laser by about one Raman time constant as can be seen as a temporal delay between peaks in Fig. 52.25.

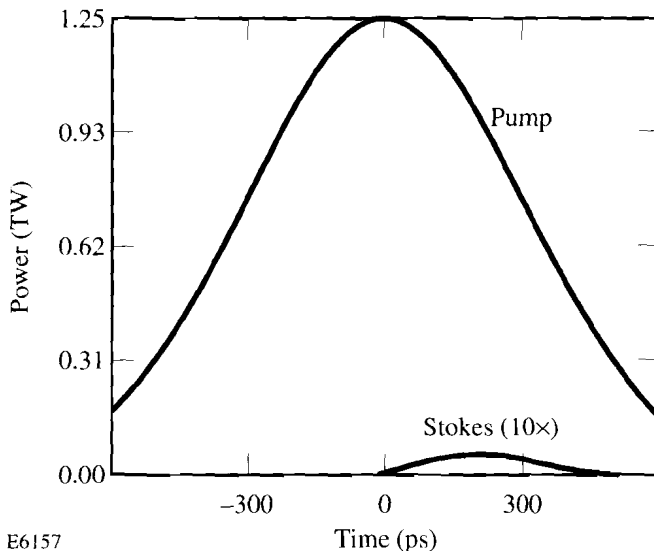
An increase in the Stokes radiation occurs for the actual shaped pulses planned for the OMEGA Upgrade laser. Using the parameters listed in Table

52.III, except for the duration over which the peak fluence occurs based on the pulse shape, a slightly greater amount of Stokes light is produced as would be expected. Although this does not present a problem, operation of the laser near threshold warrants closer examination of the detailed conditions regarding pulse-shaping, angular dispersion, and beam profile.

Table 52. III: Parameters used in transient Raman calculations.

Beam diameter	28 cm
Propagation length	18 m
Fresnel number	$\sim 10^4$
gL product (steady-state)	$\sim 25$
Laser wavelength	0.3511 $\mu$
Stokes wavelength	0.35203 $\mu$
Peak laser irradiance	$2 \times 10^9$ W/cm <sup>2</sup>
Initial Stokes irradiance	0
Laser pulse width	700 ps FWHM (Gaussian) and pulse shaped
Raman bandwidth	$7.52 \times 10^9$ sec <sup>-1</sup>
Stimulated Raman steady-state gain $g_1$	$6.76 \times 10^{-12}$ cm/W
Spontaneous Raman gain $g_2$	$6.416 \times 10^{-9}$ cm <sup>-1</sup>

E6339



E6157

Fig. 52.25

A Gaussian temporal waveform for the laser input produces a Stokes pulse that is delayed according to the SRRS response time. These results indicate that the OMEGA Upgrade laser can operate at full beam fluence while remaining below SRRS threshold.

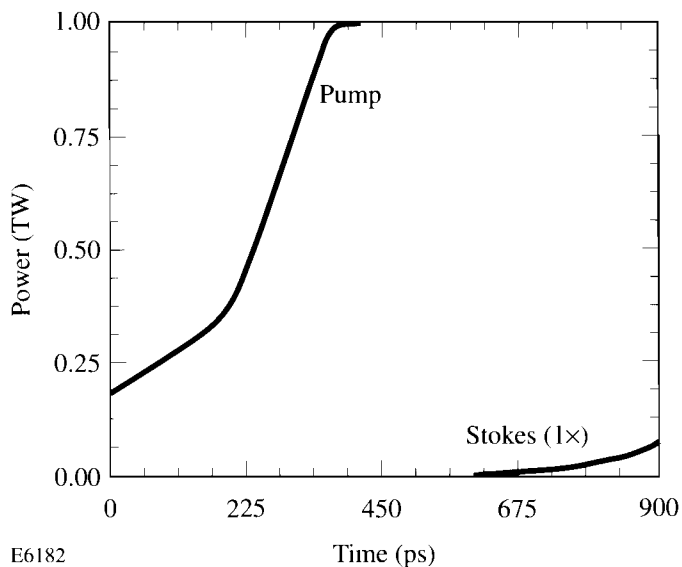


Fig. 52.26  
Raman conversion of a shaped pulse is somewhat larger than that for a Gaussian pulse because of the longer time interval at peak beam irradiance.

### Experimental Investigations

Previous experimental investigations<sup>5,6,10</sup> of Raman scattering in air involved either excessively long air paths with small beam diameters or poor beam quality, both of which make 4-D theoretical comparisons difficult, if not impossible. Poor beam quality can give rise to severe intensity variations in the near field of a beam leading to nonuniform Stokes production as well as high Stokes irradiances, which can cause premature growth of the secondary Stokes radiation. Experiments conducted under these conditions do not necessarily provide results that can be scaled to shorter paths with higher pump irradiance, such as the beamlines of the OMEGA Upgrade. In addition, aberrated pump beams often give rise to large statistical variations of the measured Raman conversion efficiency, presumably because of a greater sensitivity to gain variation for the various random noise fields.

The experimental setup, schematically illustrated in Fig. 52.27, is used to investigate Raman scattering in air within the OMEGA laser facility. The output of the 90-mm rod amplifier is directed to the prototype beamline consisting of the 15- and 20-cm SSA amplifiers, each followed by a vacuum spatial filter. Infrared laser beams, with energies between 100 J and 400 J, a beam diameter of 18 cm, and a 700-ps to 750-ps (FWHM) pulse width, are frequency converted to produce between 50 J to 150 J of UV ( $\lambda = 351$ -nm) laser light. The frequency-tripled light is characterized with near-field photography and calorimetry. The UV beam is transported along an air path of 45 m and directed to a diagnostic station consisting of a near-field camera, a one-dimensional (1-D) spectrometer, and a 2-D imaging spectrometer. The light propagated to the 1-D spectrometer is phase converted with a UV distributed phase plate (DPP) to provide uniform sampling of the near field at the slit of the spectrometer without creating high irradiance, which can cause scattering mechanisms within the diagnostic itself.

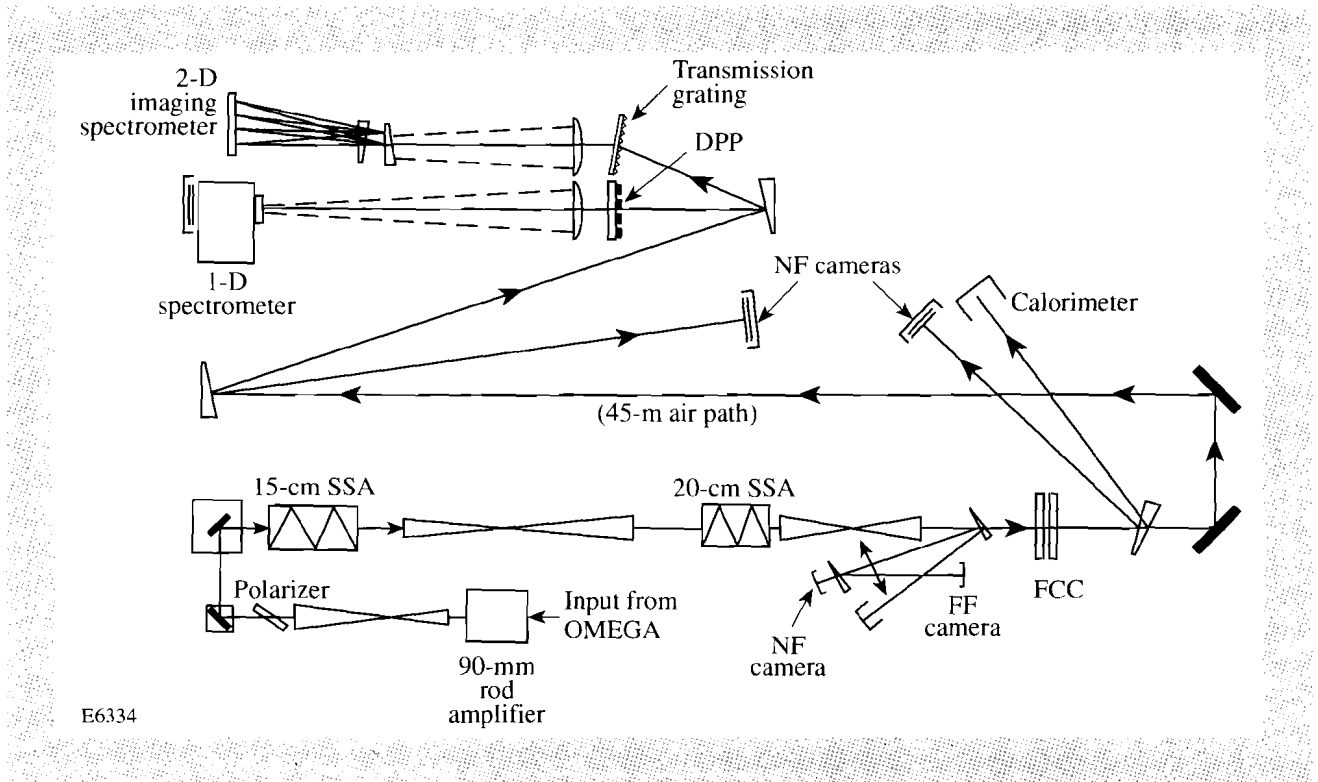


Fig. 52.27

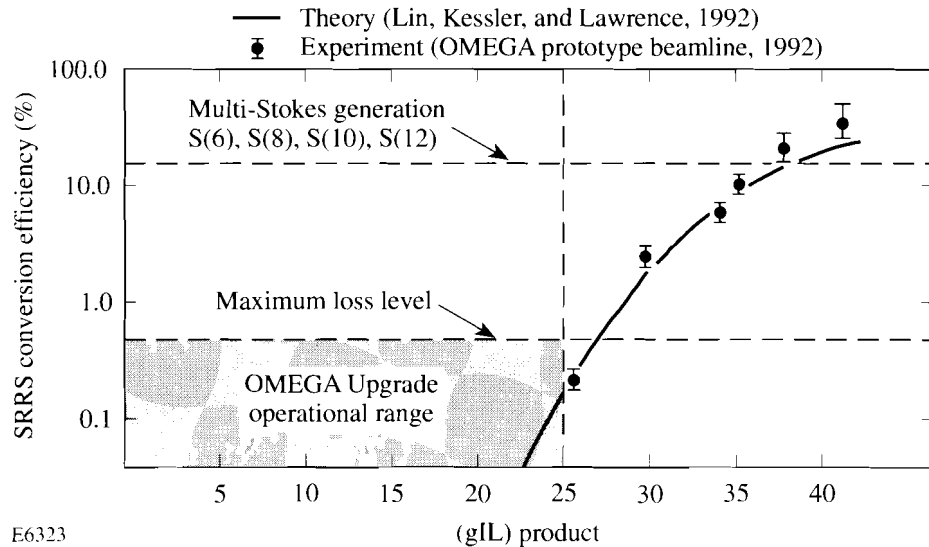
The experimental layout used to study SRRS in air consisted of a frequency-tripled SSA beamline and several laser-beam diagnostics. The diagnostics included near-field photography and calorimetry, as well as 1-D and 2-D far-field spectroscopy using diffractive optics. The 1-D grating spectrometer possessed four to five orders of magnitude in dynamic range to cover a gIL range of between 15 and 40.

The 2-D spectrometer is constructed with a UV transmission grating (1800 grooves/mm) followed by a 5-m lens, which together provides a 1-cm/nm separation of the 2-D pump and Stokes beams. The beam profile and spectra are all recorded on Kodak 4421 Aerographic film.

The results of converting a UV laser pump to Stokes light, over a (gIL) product range of 5–40, are shown in Fig. 52.28. The solid theoretical curve is generated from the SRRS code using the measured intensity distribution at the input to the Raman air path. This takes into account the actual intensity nonuniformities, but does not include the cumulative phase-front errors caused by the multi-element optical system producing the infrared laser beam. The dominant nonuniformity is a slowly varying edge-peaked profile.

An excellent agreement between the theoretical predictions and experimental results is shown in Fig. 52.28. The error bars for the two highest values for Raman conversion are large because of a vignetting of the Stokes beam prior to it reaching the slit of the spectrometer. A uniform Stokes beam, consisting of fine speckle, is expanded to a near-field beam diameter greater than that of the laser pump for gIL values greater than 35. The dynamic range of the 1-D spectrometer covers four to five orders of magnitude, making it possible to accurately compare

the experimental results to theoretical predictions, both well below and well above SRRS threshold. For gIL values of 5 A to 15 A, zero value for the Stokes light was recorded, placing an upper bound on the measurement. Reproducibility of this upper-bound measurement, together with six data points representing gIL products of between 25 and 40, provides excellent confidence in the theoretical modeling. These results indicate that it is possible to use detailed diffraction analysis to investigate the dependence that Raman conversion has on variations in pulse shape and beam profile.



E6323

Fig. 52.28

The experimental results for Raman conversion are in excellent agreement with the 4-D SRRS code developed within GLAD. The OMEGA Upgrade laser system is designed with an ultraviolet propagation path short enough to limit SRRS conversion to less than 1/2% of the total energy. Specific limits of beam profile and temporal pulse shape can be determined by use of the new SRRS code.

These experimental results also show a Stokes production that is significantly different than that of previous investigations. The S(8) and S(10) Stokes,  $\lambda = 9.39 \text{ \AA}$  and  $11.38 \text{ \AA}$ , respectively, are observed first, are nearly equal in strength, and dominate all other Stokes well past the 1% threshold. Above 10% Raman conversion the S(6) and S(12) Stokes,  $\lambda = 7.41 \text{ \AA}$  and  $13.36 \text{ \AA}$ , respectively, appear; however, they remain below the S(8) and S(10) Stokes up to a gIL product of 40, which is approximately where 50% of the laser pump converts to Raman light. Previous experiments had shown secondary Stokes, antiStokes, and other molecular transitions. It is likely that beam nonuniformities present in the pump beam, for previous experiments, caused high-irradiance Stokes light. High irradiances caused by nonuniform pump and strong spatial correlation of the Stokes lead to gIL products that exceed secondary threshold. It appears that good beam quality leads to uniformly distributed Raman speckle and less complicated Stokes production mechanisms.

Both the theoretical predictions and experimental results indicate that the beamline of the OMEGA Upgrade laser system will generate low levels of SRRS over its nominal operating conditions.

### Summary and Conclusion

A 4-D model of the effects of transient Raman scattering in the atmosphere has been incorporated into a general laser-system code. The model includes spontaneous and stimulated Raman scattering and accurately treats diffraction propagation and general laser intensity and phase distributions. The results presented here are preliminary and considerable work remains to characterize the OMEGA Upgrade laser system over an extended range of operating conditions. However, both theoretical and experimental results indicate that the level of Raman conversion in air will be acceptable over the full range of operating conditions. Further studies will seek to determine the limits of system energy, pulse width, and beam quality.

### ACKNOWLEDGMENT

This work was supported by the U.S. Department of Energy Office of Inertial Confinement Fusion under agreement No. DE-FC03-85DP40200 and by the Laser Fusion Feasibility Project at the Laboratory for Laser Energetics, which is sponsored by the New York State Energy Research and Development Authority and the University of Rochester.

### REFERENCES

1. GLAD is a proprietary product of Applied Optics Research, Tucson, AZ.
2. M. G. Raymer and J. Mostowski, *Phys. Rev. A* **24**, 1980 (1981).
3. C.-S. Wang, *Phys. Rev.* **182**, 482 (1969).
4. R. L. Carmen *et al.*, *Phys Rev. A* **2**, 60 (1970).
5. M. A. Henesian, C. D. Swift, and J. R. Murray, *Opt. Lett.* **10**, 565 (1985).
6. M. D. Skeldon and R. Bahr, *Opt. Lett.* **16**, 366 (1991).
7. R. H. Hardin and F. D. Tappert, *SIAM Rev.* **15**, 423 (1973).
8. G. N. Lawrence, "Optical Modeling," in *Applied Optics and Optical Engineering XI*, edited by R. R. Shannon and J. C. Wyant (Academic Press, New York, 1992), pp. 125-200.
9. M. D. Feit and J. A. Fleck, Jr., *J. Opt. Soc. Am. B* **7**, 2048 (1990).
10. N. A. Kurnit *et al.*, "Raman Scattering of Variable-Bandwidth KrF Laser Radiation in Long Air Paths," in *Conference on Lasers and Electro-Optics 1992 Technical Digest Series, Volume 12*, Anaheim, CA, 10-15 May 1992, paper CFA3.